2020 59th IEEE Conference on Decision and Control (CDC)
Jeju Island, Republic of Korea, December 14-18, 2020

Micro-scale 2D chiplet position control: a formal approach to policy design

Ion Matei, Johan de Kleer, Christoforos Somarakis, Anne Plochowietz and John S. Baras

***Abstract*— We address the problem of 2D position control of micro-objects (chiplets) immersed in fluid. An electric field, shaped by an array of electrodes, is used to transport and position chiplets using dielectrophoretic forces. We use a lumped, 2D, capacitive based (nonlinear) motion model to first learn a bi-modal control policy. The learning process is based on optimization featuring automatic differentiation. Next we formally prove that this policy can be generalized. The spatial dependency of the capacitances are estimated using detailed electrostatic COMSOL simulations. The results shown in this paper show that the realization of a system that can digitally convert a design directly to a physical placement of micro-chips is feasible.**

I. Introduction

Our goal is to design and build a printer system for assembling micro-objects into engineered patterns. Throughout this paper we will use chiplets, particles and micro-objects as interchangeable notions. The assembly into desired patterns is based on a feedback control loop that tracks the particles and makes corrections to their positions until the desired pattern is achieved. In [10], [9] we demonstrated a micro-particle control scheme where the actuation was done using periodic spiral-shaped electrodes. The electrodes are connected through wires to a DAC power source that sets the electrodes electric potentials. The spiral-based experimental setup allows for radial chiplet motion only, and does not scale to large number of electrodes (e.g., in the thousands) due to wiring challenges. In this paper we describe a 2D control policy where the actuation is done using an electrostatic actuator array. The photo-transistor based array is optically addressed to enable dynamic control of the electrostatic energy potential and manipulate the position of small objects [17]. The system uses dielectric fluids (e.g., Isopar-M) and supports both electrophoretic (EP) and dielectrophoretic (DEP) forces.

In this paper, we design control policies (i.e., electrodes potential assignments) that move chiplets in desired final positions. We use optimization algorithm featuring automatic differentiation to first learn these policies. The optimization cost function is numerically approximated using ideas from uncertainty quantification theory and in particular using Gauss-Hermite quadrature rules [4] to accurately approximate expectations. In addition, we formally prove that these policies generalize using a capacitive based, chiplet dynamical model.

Ion Matei, Johan de Kleer, Christoforos Somarakis and Anne Plochowietz are with the Palo Alto Research Center, Inc. (PARC). John S. Baras is with the University of Maryland, College Park.

This material is based in part upon work supported by the Defense Advanced Research Projects Agency (DARPA) under Agreement No. HR00111990027.

Paper structure: In Section II we describe the experimental setup for controlling the chiplets. Section III introduces the capacitance-based dynamical model for the particle 2D-motion, and the COMSOL model used to learn the capacitances between the particles and electrodes. In Section IV we use an optimization based approach the learn a control policy and formally prove that this policy generalizes. Section V makes a comparison of our results with the state of the art and we end the paper with some conclusions in Section VI.

II. Experimental setup

The experimental setup diagram is shown in Figure 1. The system has three hardware devices and four software modules. The hardware objects include: an imaging module and a high speed camera for tracking the chiplet locations, an array of electrodes to generate a dynamic potential energy landscape for manipulating objects with both DEP forces, and a video projector to actuate the array based on predefined patterns. The software modules include: a module for image processing that estimates the chiplet positions, a planning module that generates desired trajectories based on an objective function, a control module that compares the desired chiplet positions with the current positions and generates input signals to minimize the error between them, and an image selection/generation module that maps the control inputs to images that are projected on the array. The projected images activate or deactivate electrodes, as indicated by the control inputs. The system uses an array of

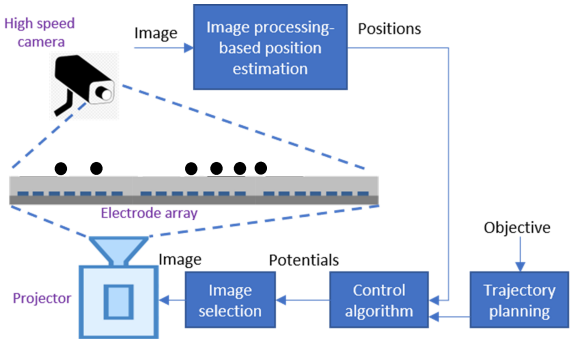

Fig. 1. Diagram of the experimental setup: a high speed camera tracks the chiplet positions that are transmitted to the control module. A planning module generates desired trajectories based on an objective function. The desired control inputs (electrode potentials) are converted into images that are projected on the array.

electrodes to generate a dynamic potential energy landscape for manipulating objects with both DEP and EP forces. The video projector is used to address each photo-transistor

978-1-7281-7447-1/20/$31.00 ©2020 IEEE

controlled electrode.More technical details about the experimental setup can be found in [1], [17]. The control objective is to design actuation algorithms and control strategies for manipulating chiplets from random to ordered patterns.

III. Dynamical model

In what follows we describe a 2D model for the chiplet motion under the effect of the potential field induced by the electrode array. The model is for one chiplet only and omits possible interactions when chiplets get close the each other.

The result of applying electric potentials to the electrodes is the generation of dielectrophoretic and electrophoretic forces that act on the chiplets. A viscous drag force proportional to the velocity[1] opposes the chiplet's motion. Due to the negligible mass of the chiplet, acceleration is ignored. It follows that the dynamical model for the chiplet model can be described by:

$$\mu\dot{x} = F_x(x,y) \tag{1}$$

$$\mu\dot{y} = F_y(x,y), \tag{2}$$

where (x,y) denotes the chiplet position measured at its center of mass, μ is the fluid dependent viscous coefficient, and $F_x(x,y)$ and $F_y(x,y)$ are projections on the x and y axis, respectively of the force induced by the potential field. We express the forces F_x and F_y as functions of the potential energy of the chiplet. We compute the potential energy by using a capacitive-based electrical circuit that lumps the interaction between the electrodes and the chiplet. Such a circuit is shown in Figure 2, where only one row with five electrodes of the array is depicted. The chiplet and the electrodes act as metal plates; hence the capacitances of these capacitors are dependent on the chiplet position. As expected, the maximum values are attained when the chiplet's position maximizes the overlap with the electrodes. To simplify the analysis, we consider the low frequency region only, where the dielectric constant is not frequency dependent. The forces F_x and F_y

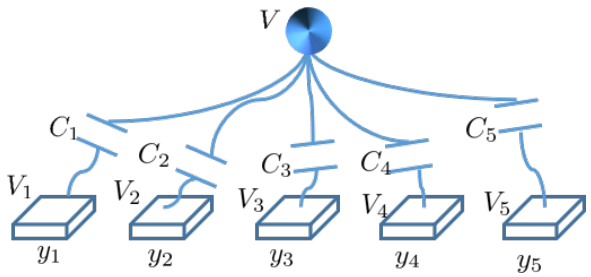

Fig. 2. Capacitive-based model describing the interaction between chiplets and electrodes.

can be expressed as $F_x(x,y) = \frac{\partial U}{\partial x}(x,y)$ and $F_y(x,y) = \frac{\partial U}{\partial y}(x,y)$, where $U(x,y)$ is the potential energy of the chiplet, given by $U(x,y) = \frac{1}{2}\sum_{i=1}^{N} C_i(x,y)[V_i - V(x,y)]^2$, where $C_i(x,y)$ is the capacitance between the chiplet and electrode i, V_i is the electric potential of electrode i, $V(x,y)$ is the electric potential of the chiplet assumed uniformly distributed across the chiplet, and N is the number of actuated electrodes. In the potential energy expression, we ignore the electrophoretic effects found negligible. The chiplet potential can be explicitly computed in terms of the electrode potentials, by solving for the voltages and currents in the electrical circuit shown in Figure 2. In particular the steady state chiplet potential is given by $V(x,y) = \frac{1}{\sum_{i=1}^{N} C_i(x,y)} \sum_{i=1}^{N} C_i(x,y)V_i$.

Feedback control design requires explicit expressions for the capacitances between the chiplet and electrodes. We learn the capacitance model using high fidelity COMSOL simulations. For symmetric chiplets (e.g., beads) assuming the electrodes are symmetric also, the capacitances are estimated by simulating a 2-dimensional electrostatic COMSOL model. This implies that the capacitance function is of the form $C_i(\eta) = C(\|\eta - \eta_i\|)$, where $\eta^T = [x,y]$ denotes the chiplet position, and $\eta_i^T = [x_i, y_i]$ is the fixed position of electrode i. The COMSOL model includes geometry and material properties of the chiplet, the electrode array and the isopar-M solution.

The COMSOL simulations do reflect the field distortion when the chiplet approaches the electrode. The COMSOL electrostatic model has as parameters, the diameter of the sphere, the electrode dimensions, the dielectric fluid constant ($\varepsilon = 2$) and the positions and material of the sphere and electrode. We fix the chiplet height ($z = 5\mu m$) and vary its position on the x-axis over the interval $[-1mm, 1mm]$. Note that due to the size of the chiplet versus the size of the electrodes, fringe effects (electric field distortions at the edges) are significant. Off-line simulations were performed for a range of chiplet positions: $x \in [-1mm, 1mm]$ and $z = 5\mu m$. The capacitances between the electrode and the chiplet were evaluated for all considered positions. We parameterized the capacitance function using error functions: $C(\xi) = \sum_{i=1}^{m} a_i \left[\Phi\left(\frac{\xi+\delta}{c_i}\right) - \Phi\left(\frac{\xi-\delta}{c_i}\right)\right]$, where $\Phi(\xi) = \frac{1}{\sqrt{\pi}}\int_{-\xi}^{\xi} e^{-t^2} dt$ is the error function, ξ is the distance between the center of the sphere and the electrode center assumed at the origin, a_i and $c_i > 0$ are positive scalars, and δ is half of the electrode pitch, i.e., 10 μm in our example. Figure 3 depicts $C(\xi)$, the capacitance between the chiplet and the electrode as a function of the chiplet horizontal position, where the numerical values were fitted on the error function parameterization. We can map the 1D model to a 2D model by using the transformation $\xi \to \sqrt{x^2+y^2}$, which results in a capacitance function $C(x,y) = \sum_{i=1}^{m} a_i \left[\Phi\left(\frac{\sqrt{x^2+y^2}+\delta}{c_i}\right) - \Phi\left(\frac{\sqrt{x^2+y^2}-\delta}{c_i}\right)\right]$.

IV. Feedback Control

To enable generalizability and tractability, we use a mean field like approximation of the dynamical model, where instead of considering a discrete distribution of the array potentials, we assume a continuous distribution. Under this assumption, we show that a bi-modal control policy, where the voltage distribution shifts polarity just in front of the chiplet does indeed induce chiplet motion to a desired direction. We start with the 1D case and show how this is extended to the 2D case. We first derive the control policy by solving a

[1]The drag force is proportional to the velocity in non-turbulent flows, that is, when the Reynolds number is small.

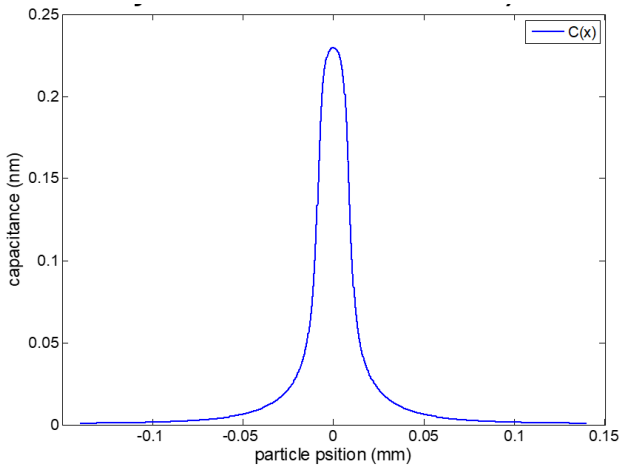

Fig. 3. Capacitance function fitted with training data generated by COMSOL simulations.

regression problem in terms of the electrodes voltages, where the key idea is the use of automatic differentiation to compute the gradients of the chiplet potential function. We next show that this policy can be generalized.

A. From micro to macro model

The intuition behind going from a discrete representation to a continuous one can be seen in the expression of the chiplet potential $V(x) = \frac{1}{\sum_{i=1}^{N} C_i(x)} \sum_{i=1}^{N} C_i(x) V_i$. In particular $V(x)$ can be interpreted as the expected value of a discrete random function $V(Y)$ over a discrete distribution $p_i(x) = C_i(x) / \sum_{i=1}^{N} C_i(x) = \tilde{C}_i(x)$. The mass function $p_i(x)$ can be interpreted as a conditional probability $p_i(x) = Pr(Y = y_i | X = x)$, and hence the chiplet potential can be expressed as $V(x) = E[V(Y)|X = x]$, where $V(y)$ is a function that reflects the potential at each point y. The discrete probability distribution can be seen as a discretization of a continuous probability distribution, i.e., $p_i(x) = \int_{y_i-\delta}^{y_i+\delta} f(y|x)dy$, where y_i is the position of the i^{th} electrode and δ is half of the electrode pitch. The parameterization of the capacitance function in terms of the error functions tells us that the conditional probability density function (pdf) is a mixture of Gaussian functions. For the sphere shaped example, the mixture has only one term, and hence the capacitance is expressed as $C_i(x) = a\left[\Phi\left(\frac{x-y_i+\delta}{c}\right) - \Phi\left(\frac{x-y_i-\delta}{c}\right)\right] = 2af(y|x)$, where $f(y|x) = \frac{1}{\sqrt{2\pi\sigma^2}} e^{-\frac{(y-x)^2}{2\sigma^2}}$, where $\sigma = \frac{c}{\sqrt{2}}$. Therefore, the chiplet potential in the continuous representation can be expressed as $\bar{v}(x) = E[V(Y)|X = x]$, where Y is a continuous random variable with a Gaussian distribution, i.e., $Y \sim \mathcal{N}(X, \sigma)$, and $V(Y)$ is a function which assigns an electric potential to each point y. The potential energy can now be represented as $U(x) = aE[(V(Y) - \bar{v}(X))^2 | X = x]$, and it follows that the 1D chiplet dynamics is given by the following partial differential equation $\frac{\partial x}{\partial t} = \frac{\partial U(x)}{\partial x}$, where $U(x) = aE[(V(Y) - \bar{v}(X))^2 | X = x]$, and $\bar{v}(x) = E[V(Y)|X = x]$.

B. Optimization based control design: 1D case

We leverage the deep-learning optimization framework [7], [13] to solve a regression problem whose result is the array's electric potential distribution. We model the function that determines the allocation of the potential as a neural network (NN) with two hidden layers of size 60 and `tanh` as activation function, that is $V(y) = V(y;\beta)$, where β is the vector of parameters encompassing the weights and the biases of the NN. The objective is to maximize the chiplet position in the positive direction. For the negative direction, we change the sign of the cost function. We numerically approximate the model expectations using the Gauss quadrature rules [4], often found in the theory of generalized chaos polynomials (GPC) [12], [18], [21]. Gauss quadrature rules provide the tool to efficiently evaluate the conditional expectations. It follows that the expectation of a function of a random variable with a Gaussian distribution, can be accurately approximated using Gauss-Hermite quadrature. We have that the expectation of $V(Y;\beta)$ is given by $\bar{v}(x;\beta) = E[V(Y;\beta)|X = x] \approx \frac{1}{\sqrt{\pi}} \sum_{i=1}^{n} w_i V\left(\sqrt{2}\sigma y_i + x;\beta\right)$, where n is the number of sample points, y_i are the roots of the physicists' version of the Hermite polynomial $H_n(y)$ and w_i are associated weights given by $w_i = \frac{2^{n-1} n! \sqrt{\pi}}{n^2 [H_{n-1}(y_i)]^2}$. Similarly, the variance of $V(Y;\beta)$ can be approximated as $U(x;\beta) = E\left[(V(Y;\beta) - \bar{v}(X;\beta))^2 | X = x\right] \approx \frac{1}{\sqrt{\pi}} \sum_{i=1}^{n} w_i \left[V\left(\sqrt{2}\sigma y_i + x;\beta\right) - \bar{v}(x;\beta)\right]^2$. Hence, we have the following optimization problem:

$$\begin{aligned} \max_{\beta} \quad & \frac{\partial \hat{U}}{\partial x}(x) \qquad (3) \\ \text{s.t.:} \quad & \hat{U}(x;\beta) = \frac{1}{\sqrt{\pi}} \sum_{i=1}^{n} w_i \left[V\left(\sqrt{2}\sigma y_i + x;\beta\right) - \hat{v}(x;\beta)\right]^2 \\ & \hat{v}(x;\beta) = \frac{1}{\sqrt{\pi}} \sum_{i=1}^{n} w_i V\left(\sqrt{2}\sigma y_i + x;\beta\right) \end{aligned}$$

We use the automatic differentiation feature of Autograd [7] to evaluate the cost function which requires the computation of the partial derivative of $\hat{U}(x)$ as a function of the NN weights and biases. To solve (3) we run Adam gradient based optimization algorithm [6], for 1500 iteration with a stepsize $\alpha = 0.001$. We solved the optimization problem for $x = 0$, and a sequence of the number of sample points $n \in \{10, 20, 30, 40, 50\}$. They all resulted in the same type of control policy, as shown in Figure 4 for $n = 30$. It is a bi-modal policy that shows the sudden change in polarity just in front of the chiplet. Due to the translational symmetry of the chiplet dynamics, it is sufficient to solve the optimization problem for $x = 0$ only.

C. Proof of generalizability

In the previous section we learned a bi-modal control policy is sufficient to induce a chiplet motion in a desired direction. Here we formally prove that this policy generalizes. We summarize the main result in what follows.

Proposition 4.1: Let the function that describes the electric potential allocation be chosen as

$$V(y) = \begin{cases} V_{max} & y \le x + b \\ -V_{max} & y > x + b, \end{cases} \qquad (4)$$

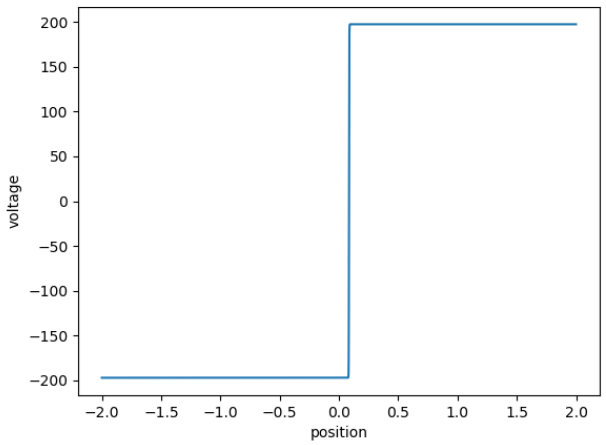

Fig. 4. Control policy obtained by solving (3) with $n = 30$ and for $x = 0$.

where V_{max} is the maximum absolute value of the electric potential. Then for $b = 0.8769\sigma$ the chiplet will move at maximum speed in the positive direction (i.e., $\dot{x} > 0$) and for $b = -0.8769\sigma$ will move the chiplet at maximum speed in the negative direction (i.e., $\dot{x} < 0$), where $\sigma = \frac{c}{\sqrt{2}}$ is the variance of the Gaussian random variable Y.

Proof: The graph of the function $V(y)$, as defined by (4) can be seen in Figure 5. The Gaussian distribution of Y

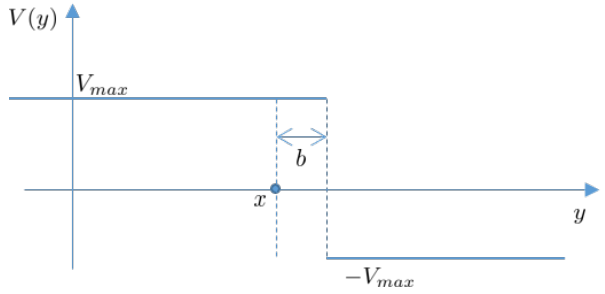

Fig. 5. Bi-modal control policy: x is the chiplet position, and the voltage polarity changes at $x+b$.

enables us to calculate the closed form expressions for $\bar{v}(x)$ and the potential energy. In particular, we have that

$$\bar{v}(x) = \int_{-\infty}^{x+b} V_{max} f(y|x)dy - \int_{x+b}^{\infty} V_{max} f(y|x)dy = V_{max}\Phi\left(\frac{b\sqrt{2}}{2\sigma}\right).$$

To evaluate the partial derivative of the potential energy, we evaluate the energy function at points x and $x+\varepsilon$, followed by the computation of the limit $\frac{\partial U(x)}{\partial x} = \lim_{\varepsilon\to 0} \frac{U(x+\varepsilon)-U(x)}{\varepsilon}$. We have that $U(x) = E[(V(Y) - \bar{v}(x))^2 | X = x] = -V_{max}^2\Phi\left(\frac{b\sqrt{2}}{2\sigma}\right)^2 + V_{max}^2$. The perturbed mean voltage is given by $\bar{v}(x+\varepsilon) = E[V(Y)|X = x+\varepsilon] = -V_{max}\Phi\left(\frac{(\varepsilon-b)\sqrt{2}}{2\sigma}\right)$, which enables us to compute the potential energy at $x+\varepsilon$, i.e., $U(x+\varepsilon) = E[(V(Y) - \bar{v}(x+\varepsilon))^2 | X = x+\varepsilon] = -V_{max}^2\Phi\left(\frac{(\varepsilon-b)\sqrt{2}}{2\sigma}\right)^2 + V_{max}^2$.

Finally, we have that

$$\frac{\partial U(x)}{\partial x} = \lim_{\varepsilon\to 0} \frac{U(x+\varepsilon)-U(x)}{\varepsilon} = \frac{4V_{max}^2\Phi\left(\frac{b\sqrt{2}}{2\sigma}\right)e^{-\frac{b^2}{2\sigma^2}}}{\sqrt{2\pi\sigma^2}}. \quad (5)$$

Expression (5) shows that $\tilde{V}(y) = -V(y)$ is a valid control policy resulting in the same energy function and induced force. Hence the maximum velocity is dictated by the maximum value of $\Phi\left(\frac{b\sqrt{2}}{2\sigma}\right)e^{-\frac{b^2}{2\sigma^2}}$. The force dependence on b is depicted in Figure 6. The force derivative in terms of b

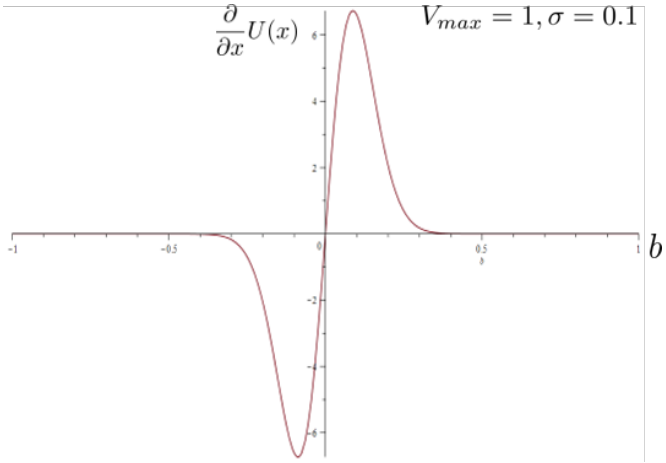

Fig. 6. Force distribution as a function of b for $V_{max} = 1$ and $\sigma = 0.1$.

as two critical points that are the solution of the equation $-\sqrt{2}\pi\Phi\left(\frac{b}{\sigma\sqrt{2}}\right)b + 2\sigma\sqrt{\pi}e^{-\frac{b^2}{2\sigma^2}} = 0$, whose solution we evaluate numerically. In particular we generated a sequence of values for σ and computed the critical points corresponding to them. We discovered that the critical points have a linear dependence on σ, namely $b^* = \pm 0.8769\sigma$. ■

The previous result shows that a bi-modal voltage distribution across the electrode does indeed ensure that the chiplet moves in the desired direction. More importantly, and not unexpectedly, it shows that only a limited number of electrodes are relevant, namely the electrodes whose positions are in the interval $[-4\sigma, 4\sigma]$. This interval cover almost entirely the non-zero segment of the force. The control policy in the continuous representation of the electrodes is practically implemented by discretizing the control policy, resulting in

$$V_i = \begin{cases} V_{max} & y_i \le x+b \\ -V_{max} & y_i > x+b, \end{cases},$$

where y_i is the position of electrode i and x is the chiplet position.

D. Extension to the 2D case

In this section we demonstrate how the previous results can be extended to the 2D case. We denote by $\boldsymbol{x} = (x_1, x_2)$ the chiplet position and by $\boldsymbol{y}^{(i)} = (y_1^{(i)}, y_2^{(i)})$ the position of electrode i. The chiplet dynamics becomes $\mu\dot{\boldsymbol{x}} = \nabla U(\boldsymbol{x})$, where μ is the viscous coefficient, and $U(\boldsymbol{x})$ denotes the

chiplet's potential energy. As is the 1D case, the potential energy is given by $U(\boldsymbol{x}) = \frac{1}{2}\sum_{i=1}^{N} C_i(\boldsymbol{x})[V_i - V(\boldsymbol{x})]^2$, where $V(\boldsymbol{x})$ denotes the chiplet electric potential, $C_i(\boldsymbol{x}) = C(\|\boldsymbol{x} - \boldsymbol{y}^{(i)}\|)$ represents the capacitance between the chiplet and electrode i a position $\boldsymbol{y}^{(i)}$, and V_i represents the potential of electrode i. Similar to the 1D case, we assume that the capacitance C_i can be represented as the un-normalized discretization of a multivariable Gaussian pdf, that is, $C_i(\boldsymbol{x}) \sim \int_{y_1^{(i)}-\delta/2}^{y_1^{(i)}+\delta/2}\int_{y_2^{(i)}-\delta/2}^{y_2^{(i)}+\delta/2} f(\boldsymbol{y}|\boldsymbol{x})d\boldsymbol{y}$, where $\boldsymbol{Y} \sim \mathcal{N}(\boldsymbol{X}, \sigma^2 I)$. The control objective is to determine a distribution for the electrode potential that moves the chiplet towards a position $\boldsymbol{x}^{(d)}$. We will consider the scenario shown in Figure 7, where the motion is paralel to the y_1 axis. This is sufficient since the potential distribution for other scenarios are derived by performing a rotational transformation as the chiplet dynamics is endowed with translational and rotational symmetries. We use the

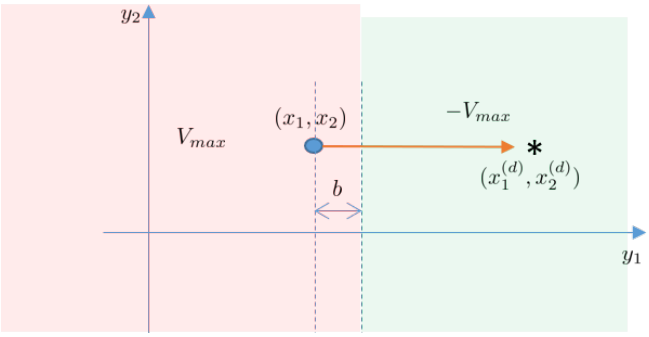

Fig. 7. Control policy in the 2D case: the objective is to move the chiplet from (x_1, x_2) to position $(x_1^{(d)}, x_2^{(d)})$

following bi-modal control policy:

$$V(\boldsymbol{y}) = V(y_1, y_2) = \begin{cases} V_{max} & y_1 \le x_1 + b, \forall y_2 \\ -V_{max} & y_1 > x_1 + b, \forall y_2 \end{cases} \quad (6)$$

The chiplet potential is computed as the mean of the potential function $V(\boldsymbol{y})$, that is $\bar{v}(\boldsymbol{x}) = E[V(\boldsymbol{Y})|\boldsymbol{X} = \boldsymbol{x}] = V_{max}\Phi\left(\frac{b\sqrt{2}}{2\sigma}\right)$. The potential energy can be computed in closed form, and is given by $U(\boldsymbol{x}) = E[(V(\boldsymbol{Y}) - \bar{v}(\boldsymbol{x}))^2|\boldsymbol{X} = \boldsymbol{x}] = -V_{max}^2\Phi\left(\frac{b\sqrt{2}}{2\sigma}\right)^2 + V_{max}^2$. To evaluate the gradient of the potential energy, we compute the partial derivatives of $U(\boldsymbol{x})$. We have that $U(x_1 + \varepsilon, x_2) = E[(V(\boldsymbol{Y}) - \bar{v}(x_1 + \varepsilon, x_2))^2|\boldsymbol{X} = (x_1 + \varepsilon, x_2)] = -V_{max}^2\Phi\left(\frac{(\varepsilon - b)\sqrt{2}}{2\sigma}\right)^2 + V_{max}^2$, where $\bar{v}(x_1 + \varepsilon, x_2) = E[V(\boldsymbol{Y})|\boldsymbol{X} = (x_1 + \varepsilon, x_2)] = -V_{max}\Phi\left(\frac{(\varepsilon - b)\sqrt{2}}{2\sigma}\right)$. It follows that

$$\frac{\partial U}{\partial x_1}(x_1, x_2) = \lim_{\delta \to 0}\frac{U(x_1 + \varepsilon, x_2) - U(x_1, x_2)}{\varepsilon} = \frac{4V_{max}^2\Phi\left(\frac{b\sqrt{2}}{2\sigma}\right)e^{-\frac{b^2}{2\sigma^2}}}{\sqrt{2\pi\sigma^2}}.$$

Similarly, we compute the partial derivative of $U(x_1, x_2)$ with respect to x_2, which turns out to be zero, that is $\frac{\partial U}{\partial x_2}(x_1, x_2) = 0$. We note that the control policy (6) generates a force on the y_1 axis only, and it has the exact expression as the force generated in the 1D case. All results determined for the 1D case concerning the choice of b to generate the maximum force hold for the 2D case, as well. Note that discretization of the ideal control policy will introduce some errors since the chiplet may not be exactly on top of an electrode. That is why, the experimental policy is based on a pattern that includes neighboring electrodes for cases when electrodes are not exactly aligned with the direction towards the desired position.

We summarize the general 2D control policy in the following result.

Proposition 4.2: Let $\boldsymbol{x}^{(0)}$ be the current chiplet position and let $\boldsymbol{x}^{(d)}$ be the desired chiplet position. Then the control policy

$$V(\boldsymbol{y}) = V(y_1, y_2) = \begin{cases} V_{max} & y_2 \le x_2^{(b)} + \frac{1}{s}\left(y_1 - x_1^{(b)}\right) \\ -V_{max} & y_2 > x_2^{(b)} + \frac{1}{s}\left(y_1 - x_1^{(b)}\right), \end{cases}$$

where $\boldsymbol{x}^{(b)} = \boldsymbol{x}^{(0)} + b\frac{\boldsymbol{x}^{(d)} - \boldsymbol{x}^{(0)}}{\|\boldsymbol{x}^{(d)} - \boldsymbol{x}^{(0)}\|}$ and $s = \frac{x_2^{(d)} - x_2^{(0)}}{x_1^{(d)} - x_1^{(0)}}$ ensure chiplet motion towards the desired position $\boldsymbol{x}^{(d)}$ for positive b and away from $\boldsymbol{x}^{(d)}$ for negative b.

Proof: The proof follows by applying a rotational transformation so that $\hat{\boldsymbol{x}}^{(0)} = R(\theta)x^{(0)}$ and $\hat{\boldsymbol{x}}^{(d)} = R(\theta)x^{(d)}$ are such that $\hat{x}_2^{(0)} = \hat{x}_2^{(d)} = 0$ and applying the policy (6). We also note that $y_2 = x_2^{(b)} + \frac{1}{s}\left(y_1 - x_1^{(b)}\right)$ is orthogonal on the line that connects $x^{(0)}$ and $\boldsymbol{x}^{(d)}$ and passes through a point $\boldsymbol{x}^{(b)}$ at a distance b from $\boldsymbol{x}^{(0)}$, on the same line. ■

V. Comparison with the state of the art

Micro- and nano-scale particle manipulation has received a significant research interest due to their significant applications in micro-fabrication, biology and medicine. In our recent work [10], [9] we showcased a micro-chiplet control policy based on a one-step model predictive control approach. The 1D model used was capacitance-based as well but the actuation mechanism was based on spiral-shaped electrodes that limited the number of simultaneously actuated electrodes. In both our current and previous results, we can deal with sizes of chiplets that can distort the electric field. A control scheme for individual and ensemble control of colloids is describe in [3]. In particular it is shown how inhomogeneous electric fields are used to manipulate individual and ensembles of colloidal particles ($1\mu m$ to $3\mu m$ diameter) in water and sodium hydroxide solutions, through electrophoresis and electroosmosis. The authors use different electrodes vs. particles scales, different medium in which the particles are immersed and different mathematical models. The authors of [16] demonstrated single particle precision and location selective particle deposition, where electrophoretic forces are the primary drive for particle (2 μm polystyrene beads) manipulation. The control scheme was based building large energy wells closed to the desired location of the nano-particles. We aim to enable sorting and placement of individual objects. We also want to manipulate asymmetric objects such as semiconductor chips, which require orientation control. Several works [22], [23] describing the control of a stochastic colloidal assembly process that drive the system to the desired high-crystalinity state are

based on a Markov-Decision Process optimal control policy. The dynamical model is based on actuator-parametrized Langevin equations. In this work, individual particles are not directly manipulated. Hence it is unclear how this approach can be used when assembling electrical circuits. Moreover, the particle size ($\approx 3\mu m$ in diameter) are small to the extent that they pose little disturbance to the electric field that is completely shaped by an actuation potentials. In addition, the time scale for achieving the desired state would make the goal of high throughput challenging to achieve. Other self-assembly control approaches [5], [14], [8] would require significant modifications to be use with our experimental system. Water based solution in which particles are immersed is a popular choice of control medium [2], [19]. In such cases, both electrophoretic forces as well as fluid motions of electro-osmotic flows are used to drive particles. A similar electrode structure to our setup in [10], [9] was used to study the effect of dielectrophoresis on cancer cells [20]. Unlike our setup, the particles are assumed small enough so that the electric field is not disturbed by their presence. Accurate control of cells, quantum dots and nano-wires bases on electroosmosis is used in [11], [15]. The authors use linear models in the electrodes potentials, and the particles effect on the electric field distribution is negligible. In the work presented in this paper, the linearity of the electrode potentials does not hold since the driving forces are primarily dielectrophoretic. In addition, the electric field is affected the chiplet position. In [24], the authors describe a dielectrophoresis-based feedback control scheme for microsphere manipulation. The authors use a simulated annealing approach for solving the optimal control problem, where they take advantage of the sphere like shape of the particle when building the system model. By comparison, our approach can accommodate rectangle shaped particles a well, and the control scheme can be easily implemented in real-time.

VI. Conclusions

We addressed the problem of digital manipulation of micro-objects using electric fields. In the experimental setup, micro sized chips immersed in dielectric fluid are manipulated by an electric field to perform fundamental operations such as transport and positioning. The actuation mechanism is implemented through an array of thousands micro-scale electrodes that shape the electric field [1]. These electrodes can be simultaneously addressed by projecting images on the array. Such an array enables fine and localized electric field shaping, hence simultaneous chiplet control is possible leading to an improved throughput. Chiplet motion is controlled by shaping the electric field, and in particular the dielectric forces induced by it. A non-linear, 2D capacitive-based model was used to formally prove that a control policy learned through optimization, does indeed determine the chiplet motion towards the desired position. A pending challenge is scaling the chiplet tracking algorithm and the real-time control scheme to controlling a large number of chiplets simultaneously. The effect of chiplet interactions must also be considered.

References

[1] E. M. Chow and et. al. Micro-object assembly with an optically addressed array. In *2017 19th International Conference on Solid-State Sensors, Actuators and Microsystems (TRANSDUCERS)*, pages 682–685, June 2017.

[2] C. F. Edman and et. al. Electric field directed assembly of an ingaas led onto silicon circuitry. *IEEE Photonics Technology Letters*, 12(9):1198–1200, Sept 2000.

[3] T. D. Edwards and M. A. Bevan. Controlling colloidal particles with electric fields. *Langmuir*, 30(36):10793–10803, 2014. PMID: 24601635.

[4] G. H. Golub and J. H. Welsch. Calculation of gauss quadrature rules. Technical report, Stanford, CA, USA, 1967.

[5] M. Grzelczak, J. Vermant, E. M. Furst, and L. M. Liz-Marzán. Directed self-assembly of nanoparticles. *ACS Nano*, 4(7):3591–3605, 2010. PMID: 20568710.

[6] D. P. Kingma and J. Ba. Adam: A method for stochastic optimization. *http://arxiv.org/abs/1412.6980*, 2014.

[7] D. Maclaurin, D. Duvenaud, and R. P. Adams. Autograd: Effortless gradients in numpy. In *ICML 2015 AutoML Workshop*, 2015.

[8] M. Mastrangeli, F. Schill, J. Goldowsky, H. Knapp, J. Brugger, and A. Martinoli. Automated real-time control of fluidic self-assembly of microparticles. In *Robotics and Automation (ICRA), 2014 IEEE International Conference on*, pages 5860–5865, May 2014.

[9] I. Matei and et. al. Towards printing as an electronics manufacturing method: Micro-scale chiplet position control. In *2017 American Control Conference (ACC)*, pages 1549–1555, May 2017.

[10] I. Matei and et. al. Micro-scale chiplets position control. *Journal of Microelectromechanical Systems*, 28(4):643–655, Aug 2019.

[11] P. P. Mathai, P. T. Carmichael, B. A. Shapiro, and J. A. Liddle. Simultaneous positioning and orientation of single nano-wires using flow control. *RSC Adv.*, 3:2677–2682, 2013.

[12] A. O'Hagan. Polynomial chaos: A tutorial and critique from a statistician's perspective. Technical report, University of Sheffield, UK, may 2013.

[13] A. Paszke and et. al. Automatic differentiation in PyTorch. 2017.

[14] J. A. Paulson, A. Mesbah, X. Zhu, M. C. Molaro, and R. D. Braatz. Control of self-assembly in micro- and nano-scale systems. *Journal of Process Control*, 27:38 – 49, 2015.

[15] R. Probst, Z. Cummins, C. Ropp, E. Waks, and B. Shapiro. Flow control of small objects on chip: Manipulating live cells, quantum dots, and nanowires. *IEEE Control Systems*, 32(2):26–53, April 2012.

[16] F. Qian and et. al. On-demand and location selective particle assembly via electrophoretic deposition for fabricating structures with particle-to-particle precision. *Langmuir*, 31(12):3563–3568, 2015. PMID: 25314133.

[17] B. B. Rupp and et. al. Chiplet micro-assembly printer. In *2019 IEEE 69th Electronic Components and Technology Conference (ECTC)*, pages 1312–1315, May 2019.

[18] R. C. Smith. *Uncertainty Quantification: Theory, Implementation, and Applications*. Society for Industrial and Applied Mathematics, Philadelphia, PA, USA, 2013.

[19] M. T. Tolley, M. Krishnan, D. Erickson, and H. Lipson. Dynamically programmable fluidic assembly. *Applied Physics Letters*, 93(25), 2008.

[20] X. B. Wang, Y. Huang, X. Wang, F. F. Becker, and P. R. Gascoyne. Dielectrophoretic manipulation of cells with spiral electrodes. *Biophysical Journal*, 72(4):1887 – 1899, 1997.

[21] N. Wiener. The Homogeneous Chaos. *American Journal of Mathematics*, 60(4):897–936, 1938.

[22] Y. Xue, D. J. Beltran-Villegas, M. A. Bevan, and M. A. Grover. Mdp based optimal control for a colloidal self-assembly system. In *American Control Conference (ACC), 2013*, pages 3397–3402, June 2013.

[23] Y. Xue, D. J. Beltran-Villegas, X. Tang, M. A. Bevan, and M. A. Grover. Optimal design of a colloidal self-assembly process. *IEEE Transactions on Control Systems Technology*, 22(5):1956–1963, Sept 2014.

[24] J. Zemánek, T. Michálek, M. Gurtner, and Z. Hurák. Feedback-controlled dielectrophoretic micromanipulation. In *2018 International Conference on Manipulation, Automation and Robotics at Small Scales (MARSS)*, July 2018.